Hindawi
Science and Technology of Nuclear Installations
Volume 2023, Article ID 8892196, 19 pages
https://doi.org/10.1155/2023/8892196

Research Article

A New Experimental Method for the Nonlinear Modal Parameter Identification of a Pressurized Water Reactor Fuel Assembly

Chen Yang,[1] **Yan Guo**,[2] **Xiao Hu**,[1] **and Yanhong Zhang**[1]

[1]*Earthquake Engineering Research Center, China Institute of Water Resources and Hydropower Research, Beijing 100048, China*
[2]*China Nuclear Power Technology Research Institute Co., Ltd., Shenzhen, Guangdong 518026, China*

Correspondence should be addressed to Chen Yang; yangchen@iwhr.com

Received 14 December 2022; Revised 30 April 2023; Accepted 12 May 2023; Published 25 May 2023

Academic Editor: Arkady Serikov

Establishing a dynamic model that accurately describes a realistic pressurized water reactor (PWR) fuel assembly is crucial to precisely evaluate the mechanical properties of the fuel assembly in seismic or loss of coolant accidents (LOCAs). The pluck test combined with the logarithmic decrement method has been widely applied in previous studies to extract fundamental modal parameters to calibrate dynamic models. However, most previous investigations focused on the first cycle of free vibration, which is strongly affected by stiction, baseline shift, drop conditions, and high-order mode interference, leading to inaccurate results. Moreover, these traditional methods cannot be used to extract high-order modal parameters. In this work, a novel experimental method for identifying the nonlinear modal parameters of a PWR fuel assembly is proposed. First, two algorithms are adopted to decompose the free vibration. Second, the local linearized modal parameters are extracted by a single-degree-of-freedom fitting method with a sliding window. Finally, these local linearized modal parameters are summed to obtain the nonlinear relationships between the modal parameters and amplitude. The new method makes more effective use of experimental data, obtains more accurate modal parameters than the logarithmic decrement method, and is capable of extracting high-order modal parameters. In the end, the test results are fitted by a fractional polynomial, which is of great value for numerical simulations.

1. Introduction

A nuclear power plant is a clean, efficient power generation facility and occupies an increasing share of the future energy supply. The PWR core contains a large number of fuel assemblies and is the major component of nuclear power plants. The safety of the PWR core is extremely important because it is the source of fissionable material leakage. Numerical simulations can be used to effectively predict the seismic behavior of PWR cores and quantify the margin in the design methodology. The fuel assembly is simplified into a dynamic model whose dynamic characteristics need to be calibrated by experiments. Many kinds of tests exist in the literature that have studied these dynamic characteristics, such as the pluck test (or snap back test without impact) [1–4], swept sine excitation test [1, 2, 4–7], step-sine harmonic excitation test [8, 9], and broadband pseudorandom excitation test [2, 8, 9]. However, the pluck test is the easiest and most convenient method. It can be used to excite the fundamental mode response with a large amplitude, which is the characteristic amplitude in seismic or LOCAs.

As early as 1988, Queval and Brochard his collaborators [1] carried out snap back tests and sweep sine tests on full-scale mock-ups. The natural frequency and damping of the fuel assembly were analyzed as a function of the motion amplitude and hold-down force, and the effect of the fluid on the dynamic characteristics was also investigated. The snap back test results and sweep sine test results were consistent with each other. Subsequently, Flamand et al. [10] observed that the drop conditions of pluck tests lead to some uncertainties in the damping ratio calculated by the logarithmic decrement method. Two kinds of single periods were compared: the first period (between the initial displacement and first maximum value) and the first "free" period (between the first and second minimum values). In addition, Fardeau et al. [11] adopted a similar calculation method: the

first natural frequency was calculated from the period of oscillation beginning at the first zero value of the displacement, the damping was calculated from the first two peaks using the logarithmic decrement method, and the effective amplitude corresponded to the difference between the initial position before release and the final position after the test. These studies considered the softening characteristics of the fuel assembly and found that the modal parameters are related to the amplitude. With further in-depth research, scholars have carried out more in-depth thinking on the requirements of pluck tests. Collard et al. [2] and Pisapia et al. [4] found that transient excitation (bending and release or pluck test) excites more than first-order modal vibration and that the contribution of higher-order modal response is not negligible. As a result, identifications resulting from this type of test are not accurate. Moreover, Roger and Lu [3] observed that the fuel assembly oscillation decays so quickly in water that even the first cycle of vibration is hard to recognize, and the null position of the assembly motion is hard to define due to the disturbance of flowing water. To obtain accurate damping in this case, the initial displacement and first response methods (also known as the data reduction method) were developed. These aforementioned studies revealed the shortcomings of traditional pluck tests from different perspectives, but only the first few cycles of oscillation were selected for calculation, and the initial displacement was taken as the characteristic amplitude. Recently, Mitsubishi Heavy Industries Ltd. [12] calculated the eigenfrequency and damping ratio not only for the first half cycle but also for successive half cycles for more visible peaks. The free oscillation of the fuel assembly shows obvious time-varying behavior, which is not suitably solved by the classic time-invariant modal analysis method. With ongoing research, time-frequency domain analysis methods provide a powerful tool for grasping the nonlinear evolution of the modal parameters of fuel assemblies, such as the short-time Fourier transform (STFT), empirical mode decomposition (EMD), Hilbert–Huang transform (HHT), and wavelet transform [13]. The wavelet transform has the ability to extract the global and local features of nonstationary signals simultaneously. It is widely employed to solve nonstationary signal problems in engineering. To cite a few examples, Le and Argoul [14] used the continuous wavelet transform of the free responses of a mechanical system for system identification purposes. Dziedziech et al. [15] applied wavelet analysis to identify the time-variant dynamics of adaptive structures. Zhao et al. [16–18] proposed a method combining the wavelet-based frequency response function with the least-squares iterative algorithm to identify the parameters of a mass, stiffness-varying multiple-degree-of-freedom structure system. Those algorithms correctly identified the modal parameters and their evolution over time. However, these works need to be further extended to the parameter's evolution with amplitude.

Although traditional pluck tests combined with the logarithmic decrement method have been widely used in previous research, they are limited to the fundamental mode case and rarely involved in the extraction of high-order modal parameters. Furthermore, experiments show that the energy dissipation mechanics in the first half cycle of free oscillation of the fuel assembly are significantly different from those in the rest of the oscillation; as a result, the logarithmic decrement method cannot obtain sufficiently precise modal parameters (this is discussed in a subsequent paragraph). In this article, the authors develop a new algorithm that overcomes the shortcomings of the traditional logarithmic decrement method. The new algorithm is based on modal decomposition and single-degree-of-freedom (SDOF) fitting with a sliding window. The test results show that the new method yields more accurate results and shows more efficient data usage. Moreover, the new algorithm can be further extended to high-order-mode and multimode cases.

The rest of this article is organized as follows. Section 2 describes the experimental setup, and Section 3 shows the experimental data. Section 4 briefly reviews the logarithmic decrement method and data reduction method and then introduces the new algorithm step by step. Section 5 shows and compares the test results. Finally, this article is completed with a discussion and concluding remarks in Sections 6 and 7, respectively.

2. Experimental Setup

The test specimen comprised a typical PWR fuel assembly, except that the fuel rods were loaded with lead pellets with a density equivalent to that of UO_2. The lead pellets matched the mechanical characteristics of the in-core assemblies and were tightly packed by axial springs. The top and bottom nozzles of the fuel assembly were pinned to a rigid water tank. The fuel assembly was submitted to a hold-down force by compressing the leaf springs of the top nozzle. The rigid water tank was fixed onto the ground, and its stiffness was much greater than that of the fuel assembly. The distance between the fuel assembly and the internal wall of the rigid water tank was 447 millimeters (mm) in the direction of the excitation. In the perpendicular direction, this distance was 3 mm. The gaps between the fuel assembly and the internal walls of the rigid water tank are illustrated in Figure 1.

The natural frequency and damping ratio of the fuel assembly were obtained by pluck tests. The excitation was applied on the middle grid of the fuel assembly (spacer grid 6 (SG6), illustrated in Figure 2) by a bending and release system. The spacer grid motions were monitored with 11 linear variable differential transformer (LVDT) displacement transducers, which were uniformly distributed along the length of the fuel assembly. All instrumentation measurements were recorded by a fast acquisition system, which provided an adequate resolution of 1000 S/sec.

The tests were conducted in air and in still water. The initial displacements of SG6 were 6 mm, 8 mm, 10 mm, 12 mm, 15 mm, 18 mm, and 20 mm in each test, and the temperature was 20°C. The pulling was provided by a manual winch at a uniform and slow speed, and the dynamic effect was negligible. At the beginning of each test, the LVDT signal baseline drift was eliminated. When the displacement of SG6 reached the desired magnitude, the authors waited

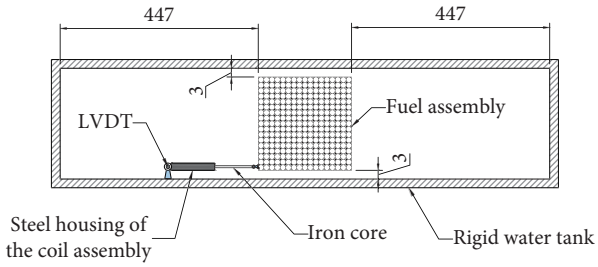

Figure 1: Gaps between the fuel assembly and internal walls of the rigid water tank (in millimeters).

for an interval of approximately 20 seconds before releasing the fuel assembly. The release of the fuel assembly was controlled by an electromagnetic chuck, and the initial speed of the fuel assembly was almost zero. Since SG6 is the center of the fuel assembly, the deformation of the fuel assembly approximates the first-order mode shape. The test facility and instruments are illustrated in Figure 2.

3. Test Data

Figure 3 shows the free oscillations of all spacer grids (marked as grids 1~11) during the 20 mm test in air and still water (other test results are omitted for brevity). The following phenomena should be considered. (1) The vibration of the fuel assembly decays faster in still water than in air due to the fluid resistance generated by the lateral motion of the fuel assembly. (2) At the tail end of the vibration, spacer grids cannot be restored to their original states due to the slippage between fuel rods and spacer grid cells. (3) Not all spacer grids start sliding synchronously, and grid 6 starts moving first and then drives adjacent grids. (4) The vibration amplitude decays rapidly in the first few cycles, especially in still water.

Figure 4 shows the initial 0.5 seconds of free oscillation during 20 mm tests in air and still water, and it is clear that grid 6 starts moving first and then drives adjacent grids. The time interval taken for grid 6 and the bottom or top grid to start moving is approximately 0.06 seconds. The initial 0.06 second oscillation has a different energy dissipation mechanism than that of the subsequent oscillations, which is a topic of interest.

4. Data Processing Method

4.1. Logarithmic Decrement Method. The logarithmic decrement (LogDec) method is a fundamental modal parameter extraction algorithm that can be used only in situations in which a structure can be well idealized as a linear elastic SDOF system. Any free vibration cycle of the linear elastic SDOF system calculates the same modal parameters by the LogDec algorithm. However, as shown in Figure 3, the vibration of the fuel assembly exhibits typical softening characteristics, and the modal parameters of the fuel assembly are related to the amplitude. As a result, the traditional LogDec algorithm that uses only the first vibration cycle gives inaccurate results.

In this paper, the vibration time history of SG6 is taken as a gradual process of nonlinear evolution of the frequency and damping ratio. The visible successive peaks and valleys were selected to define each vibration cycle T_D, for which the fuel assembly can be locally linearized as an SDOF system and solved by the LogDec algorithm. The logic behind this approach is that the nonlinear vibration time history of SG6 is dominated by the first-order mode and can be considered the sum of consecutive quasi-linear and stationary SDOF free decay response segments. This local linearization is a commonly used method for dealing with nonlinear problems. Furthermore, it is convenient to calculate the equivalent modal parameters of each segmented response by LogDec. The difference between the measured and the reconstructed signal by equivalent modal parameters is small, and the reconstructed signal has the same peak or valley value as the segmented response. These successive equivalent modal parameters form the nonlinear relationships between the natural frequency and amplitude and the damping ratio and amplitude. This process is illustrated in Figure 5: the first cycle is selected between the first two peaks, and the second cycle is selected between the first two valleys. The second cycle lags only half a period behind the first cycle. The parameters a_1, w_{n1}, and ζ_1 represent the characteristics of amplitude, natural frequency, and damping ratio for the first cycle, respectively, and the subscript numbers correspond to the cycle number.

4.2. Data Reduction Method. Due to the strong nonlinearity and large damping ratio of the fuel assembly at a large vibration amplitude, the response signals last only a few cycles, especially in still water. The LogDec method was modified and applied to the half cycle oscillation to obtain the vibration amplitude, natural frequency, and damping ratio. The mathematical formulation is expressed in (1) and (2):

$$\sqrt{1-\zeta^2}\,w_n T_{0.5D} = \pi, \tag{1}$$

$$\delta_\pi = \ln\left|\frac{y(T_{0.5D})}{y(0)}\right| = \zeta w_n T_{0.5D} = \frac{\pi\zeta}{\sqrt{1-\zeta^2}}, \tag{2}$$

where $T_{0.5D}$ is half of the damped period, calculated by successive peaks and valleys.

Instead of the full cycle adopted in the LogDec method, a half-cycle oscillation is selected in this algorithm, corresponding to local linearization on a half cycle other than a full cycle. This methodology was named the data reduction method or "initial displacement and first response method" [3, 12], as illustrated in Figure 6.

4.3. A New Algorithm Based on Modal Decomposition and SDOF Fitting with a Sliding Window (POD (svd)). A fuel assembly is a multi-degree-of-freedom structure. Generally, its free oscillation can be decomposed into several single-mode responses with initial displacements and velocities [19]:

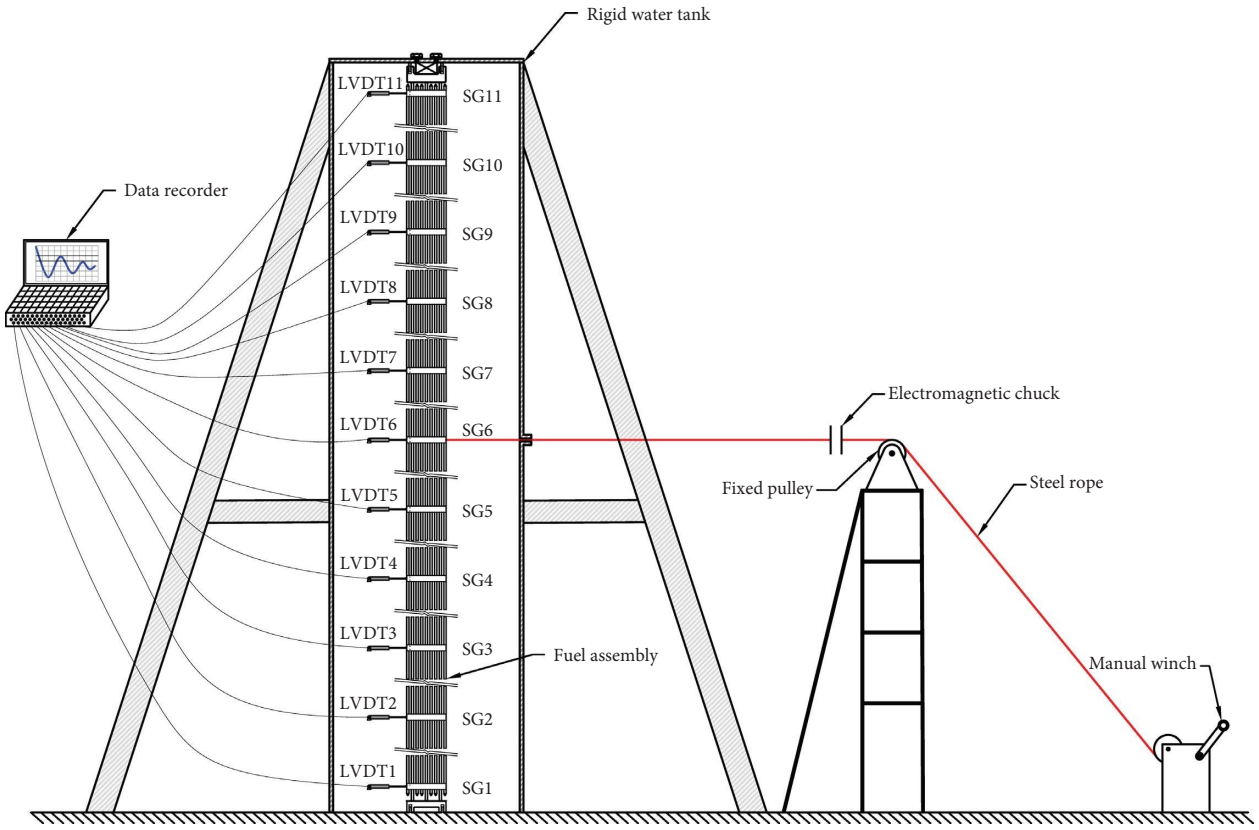

Figure 2: Configuration of the tests.

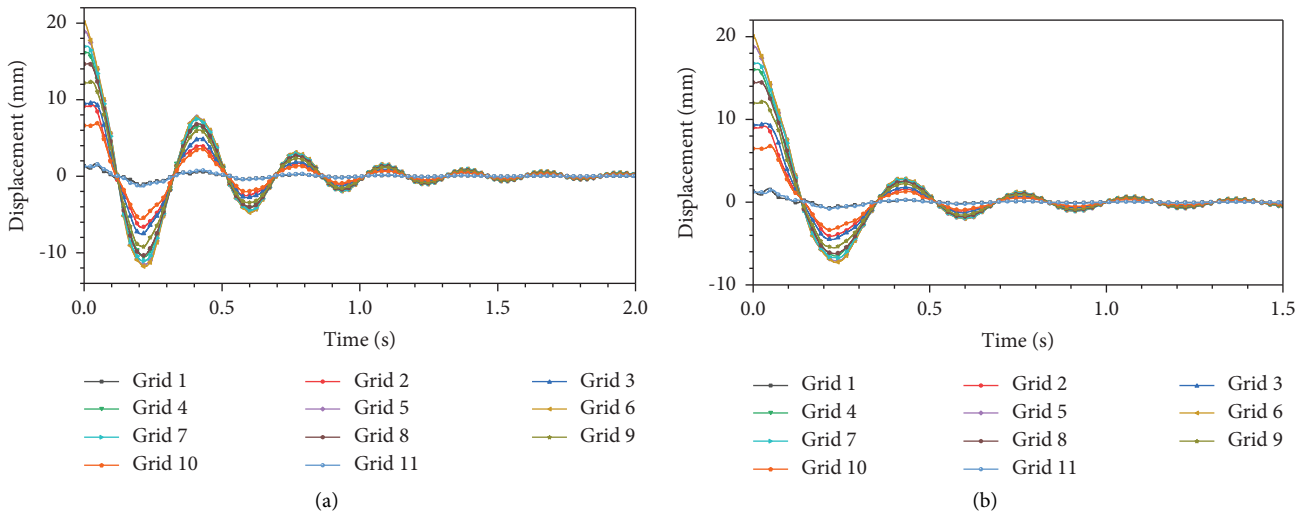

Figure 3: Free oscillation of all spacer grids: 20 mm test. (a) In air. (b) In still water.

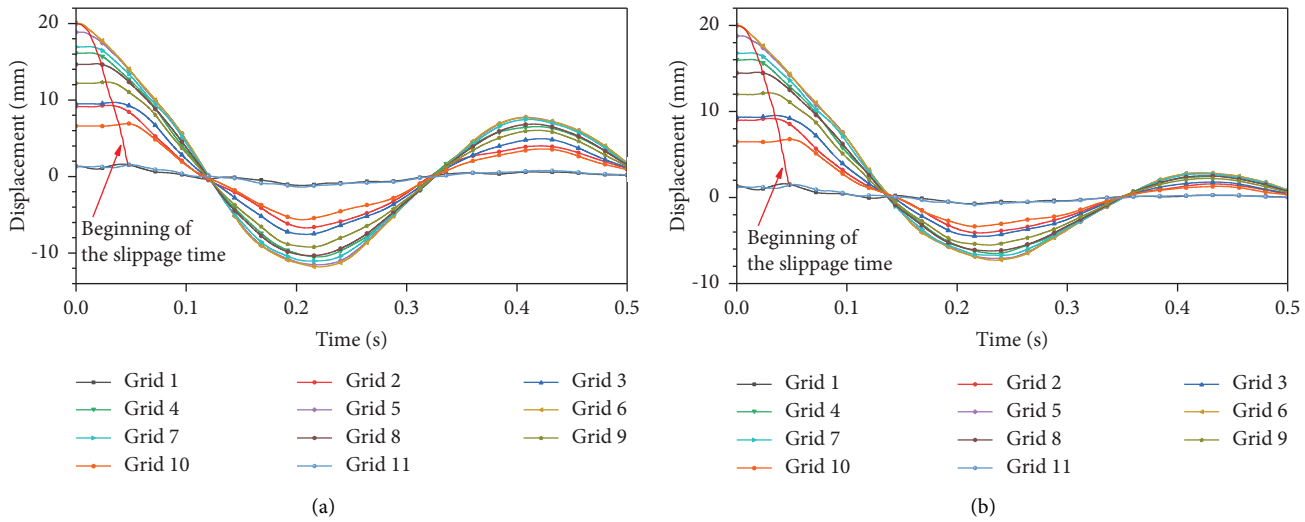

Figure 4: Beginning of the slippage time for the spacer grids: 20 mm test. (a) In air. (b) In still water.

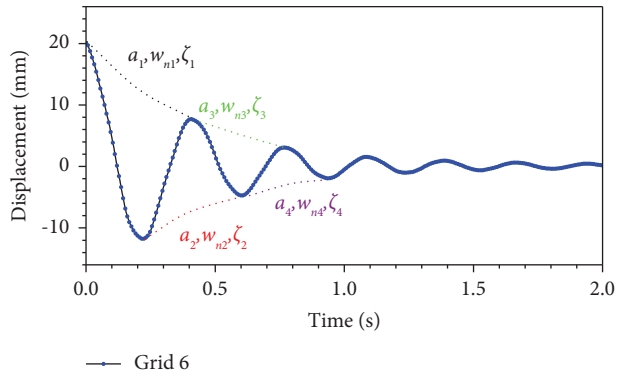

Figure 5: Schematic diagram of the LogDec method.

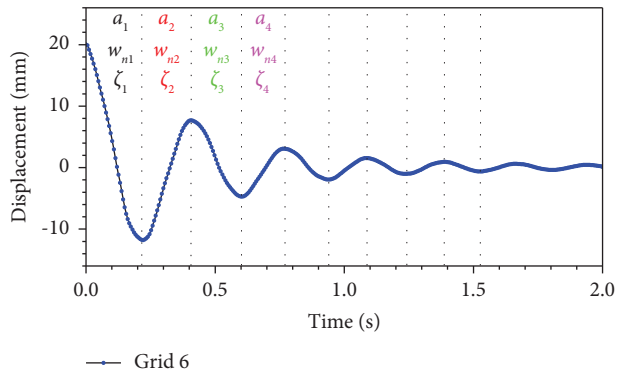

Figure 6: Schematic diagram of the data reduction method.

$$
\begin{aligned}
\mathrm{y}(t) &= \sum_{i=1}^{N} a_i e^{-\zeta_i w_{ni} t} \sin\left(\sqrt{1-\zeta_i^2}\, w_{ni} t + \theta_i\right)\psi_i,\\
a_i &= \sqrt{\left(\frac{\dot{x}_i(0) + \zeta_i w_{ni} x_i(0)}{w_{ni}\sqrt{1-\zeta_i^2}}\right)^2 + x_i(0)^2},\\
\tan\theta_i &= \frac{x_i(0) w_{ni}\sqrt{1-\zeta_i^2}}{\dot{x}_i(0) + \zeta_i w_{ni} x_i(0)},\\
\psi_i &= \begin{Bmatrix} \varphi_{1i} \\ \vdots \\ \varphi_{mi} \end{Bmatrix},
\end{aligned}
\tag{3}
$$

where N is the modal order and $\dot{x}_i(0)$, $x_i(0)$, w_{ni}, ζ_i, a_i, θ_i, and ψ_i are the initial velocity, initial displacement, natural frequency, damping ratio, amplitude, phase angle, and mode shape of the ith mode, respectively.

The fuel assembly is a strongly nonlinear system, and studies show that w_{ni}, ζ_i values are largely dependent on a_i (amplitude of the ith mode) [1, 11, 20], and ψ_i is almost independent of the vibration amplitude and considered a constant vector (this will be discussed in another paper). As a result, time-domain modal parameter estimation algorithms, such as the least-squares complex exponential (LSCE) [21, 22], Ibrahim time-domain method (ITD) [23], and eigensystem realization algorithm (ERA) [24], are not applicable to this case. The fast Fourier transform $y(t)$ into the frequency domain and the frequency-domain modal parameter estimation algorithm are also not applicable. It is impossible to construct an equation to solve the nonlinear modal parameters because the relationships between w_{ni} and a_i and between ζ_i and a_i are unknown. To solve this problem, a new algorithm is developed and divided into the following two steps: (1) single-mode response extraction and (2) nonlinear modal parameter extraction.

4.3.1. Single-Mode Response Extraction. The first and most important step is single-mode response extraction, and there are two methods that can be used to extract the single-mode response.

Algorithm 1. Extract the single-mode response by the orthogonality of the mode shape with respect to the mass matrix.

Experiments show that the mode shape of the fuel assembly remains constant regardless of the condition (in air or in still water) and the vibration amplitude. The mass matrix of the fuel assembly can be approximated by a lumped mass matrix. Based on the orthogonality of the mode shape with respect to the mass matrix, the single-mode response can be separated from $\tilde{y}(t)$ as follows:

$$
\tilde{y}_{\mathrm{mi}}(t) = \frac{{\psi_i}^T * \mathrm{M} * \tilde{y}(t)}{{\psi_i}^T * \mathrm{M} * \psi_i},
\tag{4}
$$

where $\tilde{y}(t)$ is the measured response of the spacer grids, ψ_i is the ith mode shape and is normalized by setting the maximum element as 1.0, M is the lumped mass matrix, and $\tilde{y}_{\mathrm{mi}}(t)$ is the ith separated single-mode free decay response.

Algorithm 2. Proper orthogonal decomposition.

Proper orthogonal decomposition (POD) is extremely useful in data analysis to identify the most energetic modes of a complex system [5, 25, 26]. POD, also known as singular value decomposition (SVD) and principal component analysis (PCA), is a dimensional reduction or feature extraction method. Its historical review, mathematical formulation, and physical interpretation can be found in reference papers. Here, the SVD of the response matrix is adopted and stated in equations (5) and (6):

$$
\tilde{\Psi} = \left[\tilde{y}(t_1), \cdots, \tilde{y}(t_n)\right] = \begin{bmatrix} \tilde{y}_1(t_1) & \cdots & \tilde{y}_1(t_n) \\ \vdots & \vdots & \vdots \\ \tilde{y}_{11}(t_1) & \cdots & \tilde{y}_{11}(t_n) \end{bmatrix},
\tag{5}
$$

$$
\tilde{\Psi} = \tilde{\mathrm{U}}\tilde{\mathrm{S}}\tilde{\mathrm{V}}^T,
\tag{6}
$$

where $\tilde{\Psi}$ is the response matrix $(11 \times n)$, and each column represents the displacement recorded by the 11 LVDTs at time t_i; $\tilde{U}$ is an (11×11) orthonormal matrix containing the left singular vectors; $\tilde{S}$ is an $(11 \times n)$ pseudodiagonal and semipositive definite matrix with diagonal entries containing the singular values s_k; $\tilde{V}$ is an $(n \times n)$ orthonormal matrix containing the right singular vectors; and $\tilde{V}^T$ is the transpose of $\tilde{V}$.

The temporal evolution $p_k(t)$ is given by the kth row of the matrix P (stated in (7)). The amount of energy captured by each mode can be represented by the relative magnitude of its corresponding singular value s_k.

$$
\mathrm{P} = \tilde{\mathrm{S}}\tilde{\mathrm{V}}^T.
\tag{7}
$$

To extract the single-mode response, each column of the orthogonal base matrix $\tilde{U}$ should be normalized by setting the maximum element as 1.0 (equations (8) and (9), in accordance with the LogDec algorithm applied to the free vibration of SG6). The recorded displacement $\tilde{y}(t_i)$ can be represented by a combination of several single-mode responses (equation (10)). In this test configuration, the 1st-order mode response accounts for the most energy, $\tilde{\Phi}_1$ is a good approximation of the 1st-order mode shape (singular values s_k are arranged in descending order), and $\tilde{y}_{m1}(t_i)$ is a good approximation of the 1st-order mode response (equation (11)).

$$
\tilde{U} = \left[\tilde{u}_1, \cdots \tilde{u}_k, \cdots \tilde{u}_{11}\right],
\tag{8}
$$

$$
\tilde{\Phi}_k = \frac{\tilde{u}_k}{\max\left(\left|\tilde{u}_k\right|\right)},
\tag{9}
$$

$$
\tilde{y}(t_i) = \sum_{k=1}^{N} \tilde{p}_k(t_i)\tilde{\Phi}_k,
\tag{10}
$$

$$\tilde{y}_{\mathrm{mk}}(t_i) = \tilde{p}_k(t_i) = \frac{\tilde{\Phi}_k^T * \tilde{\mathrm{y}}(t_i)}{\tilde{\Phi}_k^T * \tilde{\Phi}_k}, \tag{11}$$

where $\tilde{u}_k$ is a column of the orthogonal base matrix $\tilde{U}$; $\tilde{\Phi}_k$ is the vector obtained by normalizing the maximum value in $\tilde{u}_k$ to 1.0; and $\tilde{y}_{mk}(t_i)$ is the kth separated single-mode free decay response (redefined as $\tilde{p}_k$), which is proportional to the temporal evolution of the kth proper orthogonal modes (POMs).

Both equations (4) and (11) can be used to extract the first-order and high-order mode free decay response. However, they are different in the following aspects: (1) equation (4) assumes that the mode shape and mass matrix are known and that the orthogonality of the mode shape with respect to the mass matrix is satisfied; (2) equation (10) assumes that the free decay response can be projected onto the orthogonal base $\tilde{\Phi}_k$, which is a good approximation of the mode shape. However, the measured normal mode shape ψ_i might not satisfy this kind of orthogonality (this is affected by the mass distribution, stiffness distribution, and by the locations and amounts of sensors fixed onto the fuel assembly). Different implications of orthogonality result in different extracted single-mode free decay responses.

4.3.2. Nonlinear Modal Parameter Extraction. Once the single-mode response has been extracted, the nonlinear modal parameters can be extracted with any appropriate algorithm. In this paper, a new algorithm based on a sliding window and SDOF fitting is proposed. It is divided into the following steps: (1) omit the onset 0.06 seconds and the tail data for $\tilde{y}_{mi}$ or $\tilde{y}_{mk}$, which are severely affected by stiction (the omitted data vary from test to test, and for different kinds of fuel assemblies, the time interval of 0.06 seconds is just for illustration); (2) set the start time of the window, which can be evenly distributed over the entire vibration time range or densely distributed in the first few vibration cycles as needed; and (3) set the end time of the window (this is discussed in the next paragraph). Generally, the window length covers a full vibration cycle and depends on the variation in the modal parameters. (4) Select the data in the current window and calculate the locally linearized modal parameters by fitting the theoretical formulation of the SDOF free decay response (equation (12)). (5) The window's start time index is moved to the next point, and whether the windows cover the entire duration of the vibration is evaluated. The calculated results are summarized and form a nonlinear relationship between the modal parameters and the amplitude. The algorithm is illustrated in Figure 7, and the calculation flowchart is shown in Figure 8.

$$y_i(t) = a_i e^{-\zeta_i w_{\mathrm{ni}} t} \sin\left(\sqrt{1-\zeta_i^2}\, w_{\mathrm{ni}} t + \theta_i\right) + d_{\mathrm{ik}}, \quad t_p \le t < t_p + \Delta t, \tag{12}$$

where y_i is the SDOF free decay response; a_i, w_{ni}, and ζ_i are the characteristic amplitude, locally linearized natural frequency, and damping ratio, respectively; d_{ik} is a constant

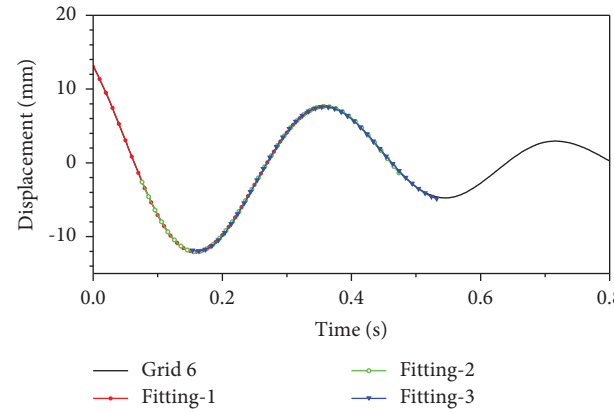

Figure 7: Illustration of the new algorithm: 3 start times and corresponding SDOF fitting results.

that compensates for the drift of the baseline; t_p is the start time of the window; and Δt is the window length.

It is worth emphasizing that the end time for the window (or the window length Δt) is difficult to determine in advance for the following reasons: (1) Δt should be consistent with w_{ni}; a smaller w_{ni} necessitates a larger Δt, and vice versa; (2) as the vibration amplitude decreases, the variation in the modal parameters gradually decreases, and Δt should increase synchronously; and (3) the larger Δt, the larger the fitting error and the stronger the smoothing effect on the locally linearized modal parameters, which cannot reveal the local characteristics of the modal parameters. However, a smaller Δt cannot reflect the consistent evolution of the modal parameters. Considering the above factors, a normalized fitting error indicator E_r is proposed, which is defined in equation (13) (the fitting error can be weighted as needed). E_r is a monotonically increasing nonlinear function of the window width Δt. Given an appropriate threshold for E_r, Δt can be calculated by the bisection iteration method.

$$\mathrm{E}_r = \frac{\sum_{j=p}^{q}\left(\tilde{\mathrm{y}}_m(t_j) - \mathrm{y}_i(t_j)\right)^2}{\sum_{j=p}^{q}\tilde{\mathrm{y}}_m(t_j)^2}, \quad t_p \le t_j < t_q, \quad \Delta t = t_q - t_p, \tag{13}$$

where $\tilde{y}_m$ is the separated single-mode free decay response ($\tilde{y}_{\mathrm{mi}}$ or $\tilde{y}_{\mathrm{mk}}$), y_i is the reconstructed response, and t_q is the end time for the window.

The SDOF fitting method has the following advantages: (1) it does not need to meet the initial zero velocity requirement; (2) it overcomes the effect of baseline drift or residual displacement; (3) the window length Δt is determined by the fitting error threshold for E_r (in the LogDec and data reduction methods, the window length is equal to the full cycle or half cycle, which is an adaptive process determined by the signal itself); and (4) the evolution of the nonlinear relationship can be densely distributed on large amplitudes as needed (setting the multiple start time index

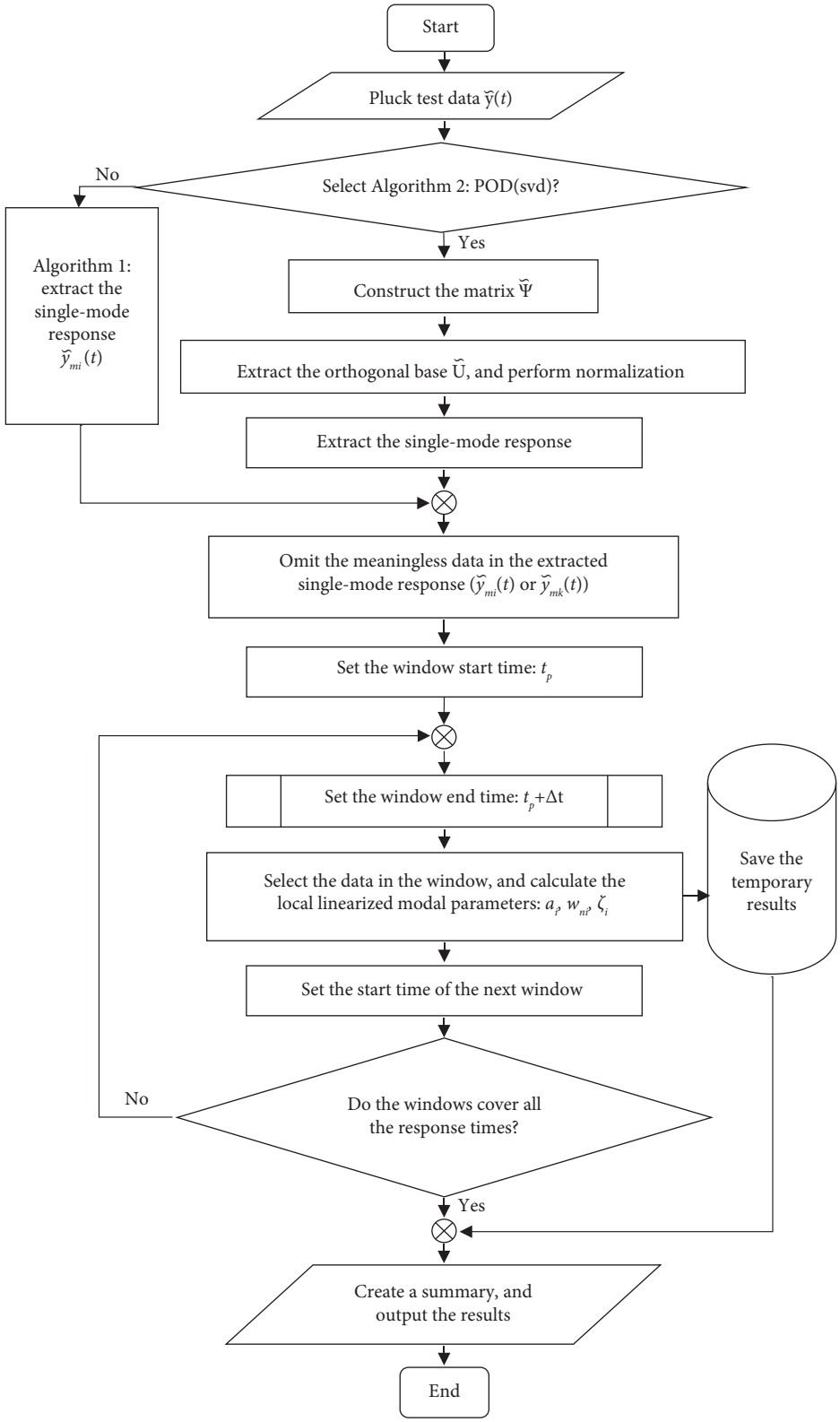

Figure 8: Flowchart for the new algorithm.

of the window in the first few cycles). These advantages are demonstrated in the test results.

5. Test Results and Comparison

5.1. Test Result Based on LogDec and the Data Reduction Method. The displacement histories for grid 6 in air and in still water are summarized in Figure 9 and selected as input data for LogDec and the data reduction methods. Typically, 20 mm test results are shown in Figures 10 and 11.

The results clearly show that (1) the attenuation of the vibration amplitude is mainly concentrated in the first two cycles of the test in air and the first cycle in still water, and (2) as the amplitude increases, the natural frequency decreases, and the damping ratio increases. The stiffness reduction for large displacement is caused by the fuel rod support condition changes (springs and dimples) and is more effective for small displacements. When the amplitude is small, the support spring force and friction between the fuel rod and support prevent any relative motion, and the energy dissipation mainly comes from material damping. For large amplitudes, sliding friction between the contact surfaces increases the structural damping, which thus consumes most of the energy. (3) The LogDec algorithm and data reduction method yield similar results, although the LogDec results are smoother. The reason is obvious: the LogDec algorithm uses full-cycle data, while the data reduction method uses only half-cycle data and has a poorer smoothing effect. This, together with the softening properties, explains the following phenomena: in Figures 10 and 11, the initial natural frequency (the natural frequency associated with the 20 mm amplitude) calculated by the data reduction method is smaller than the LogDec result, but the damping ratio shows the opposite behavior. The result calculated by the data reduction method oscillates around the LogDec result and has a large amount of scatter at low amplitude because the fuel rod is stuck by the dimple and spring clamping. (4) The natural frequency in still water is lower than that in air due to the added mass effect. The damping in still water is increased compared to that in air due to the drag forces caused by the lateral motion of the fuel assembly in the fluid. (5) The damping ratio in air gradually saturates with increasing vibration amplitude but not in still water. A possible explanation is that there is an upper limit to the frictional force between the fuel rod and grid cell. Conversely, the fluid damping force is proportional to the square of the velocity, which is proportional to the vibration amplitude, and as a result, the damping ratio in still water has no upper limit.

Figure 12 summarizes the nonlinear relationship for the first-order modal parameters versus amplitude determined by the LogDec method, and Figure 13 shows the data reduction method. The results for different initial displacements are consistent with each other. However, the LogDec algorithm results are smoother than those obtained by the data reduction method. The reasons are as stated before. At the tail end of the vibration, baseline drift and residual displacement have much more severe effects on the results of the data reduction method than LogDec. All of these factors contribute to the spread observed in the small vibration amplitude results.

5.2. Test Result Based on the POD (svd) Method. The key factor for the POD (svd) algorithm is the separation of the single-mode free decay response. However, the accuracy of the extracted single-mode response depends heavily on the mode shape accuracy and orthogonality. The data used to construct the matrix $\widetilde{\Psi}$ (in equation (5)) are critical to obtain an accurate mode shape. A normalized deformation energy ratio $\mathrm{DE}_r(t_i)$ is defined in equation (14). When $\mathrm{DE}_r(t_i)$ lies between a certain upper and lower bound, the data in the range are used to construct the matrix $\widetilde{\Psi}$. The basic idea of $\mathrm{DE}_r(t_i)$ is that (1) the start and end segment data for the vibration should be omitted as they are greatly affected by static friction; (2) when the fuel assembly passes through the equilibrium position, the data should not be used due to its poor signal-to-noise ratio (SNR). The sensitivity analysis shows that the first orthogonal base $\widetilde{\Phi}_1$ is not sensitive to the upper and lower bounds of $\mathrm{DE}_r(t_i)$, and the appropriate lower and upper bounds are 0.05 and 0.6, respectively. The calculated first orthogonal base $\widetilde{\Phi}_1$ and the benchmarking mode shape (obtained by additional experimental modal analysis) are both shown in Figure 14. It is clearly shown that the $\widetilde{\Phi}_1$ values in different tests coincide with each other, which confirms the invariance of the mode shape to some extent.

$$\mathrm{DE}_r(t_i) = \frac{\widetilde{y}(t_i)^T * \widetilde{y}(t_i)}{\widetilde{y}(t_0)^T * \widetilde{y}(t_0)}, \tag{14}$$

where $\widetilde{y}(t_i)$ is the displacement time history of grid 6 in each test and t_0 is the start time.

Taking the 20 mm test as an example, the first-order modal response extracted by equation (4) (marked as benchmarking) and equation (11) (marked as POD (svd)) is shown in Figure 15, along with the grid 6 displacement time history. It is obvious that (1) the three free decay responses are very similar except for the initial 0.06 seconds. The reason for this phenomenon is that SG6 starts moving first and then drives adjacent grids. The contact interface for the fuel rod and spacer grids changes from static friction to dynamic friction. Therefore, the initial 0.06 seconds of vibration has a different energy dissipation mechanism from that of subsequent vibrations. (2) The POD (svd) algorithm results are very similar to the benchmarking results. An appropriate explanation is that the lumped mass matrix can be approximated as a unit diagonal matrix multiplied by a constant, which means that the two kinds of orthogonality are essentially the same. (3) The initial elastic deformation of the fuel assembly closely approximates the 1st-order mode shape. Therefore, the displacement time history for grid 6 matches the extracted 1st-order mode response. However, if the grid is not carefully selected to impose an initial displacement, the multiorder modal response is excited, and the requirements of the LogDec and data reduction methods cannot be fulfilled.

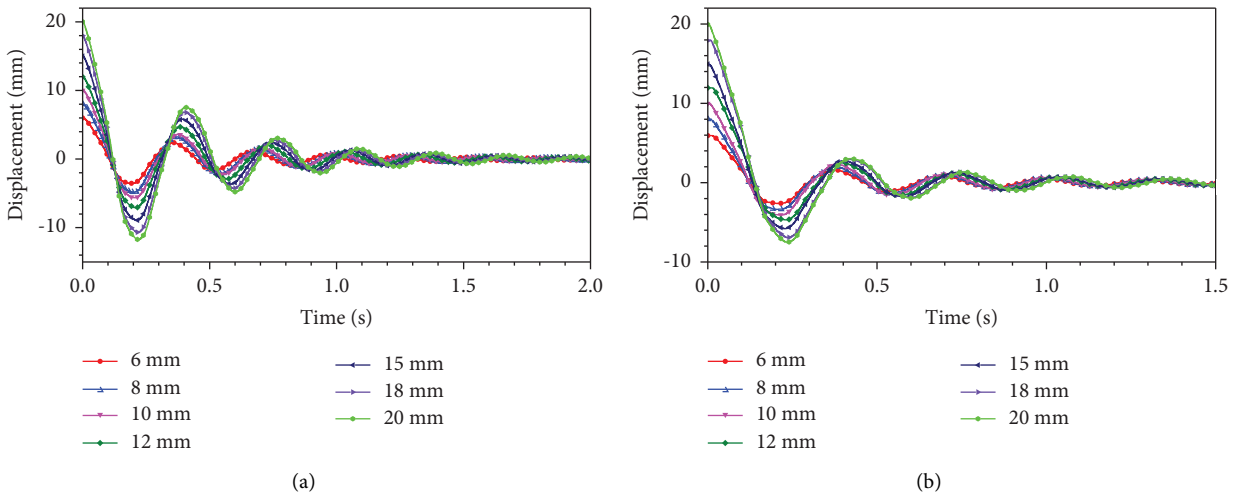

Figure 9: Summary of free oscillation of spacer grid 6. (a) In air. (b) In still water.

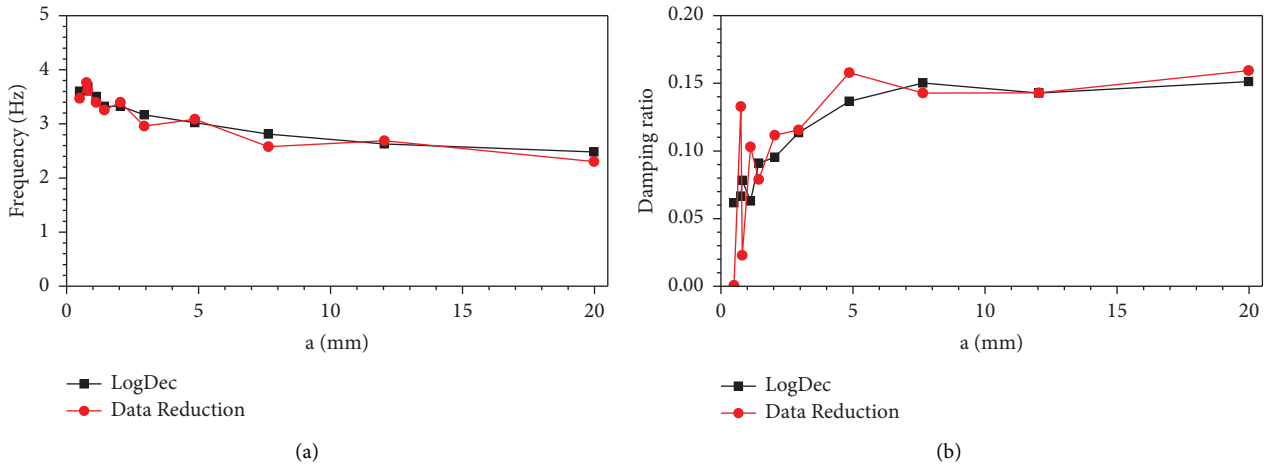

Figure 10: 1st-order natural frequency versus amplitude relationship and damping ratio versus amplitude relationship: 20 mm test in air. (a) Natural frequency. (b) Damping ratio.

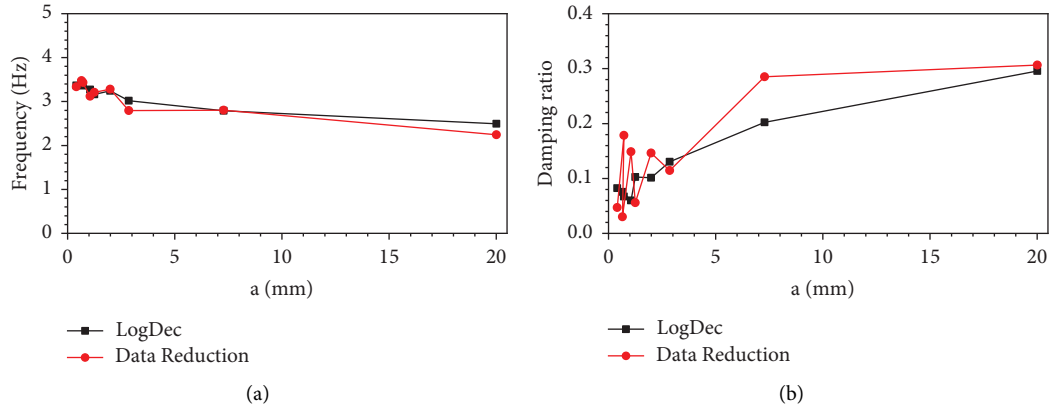

Figure 11: 1st-order natural frequency versus amplitude relationship and damping ratio versus amplitude relationship: 20 mm test in still water. (a) Natural frequency. (b) Damping ratio.

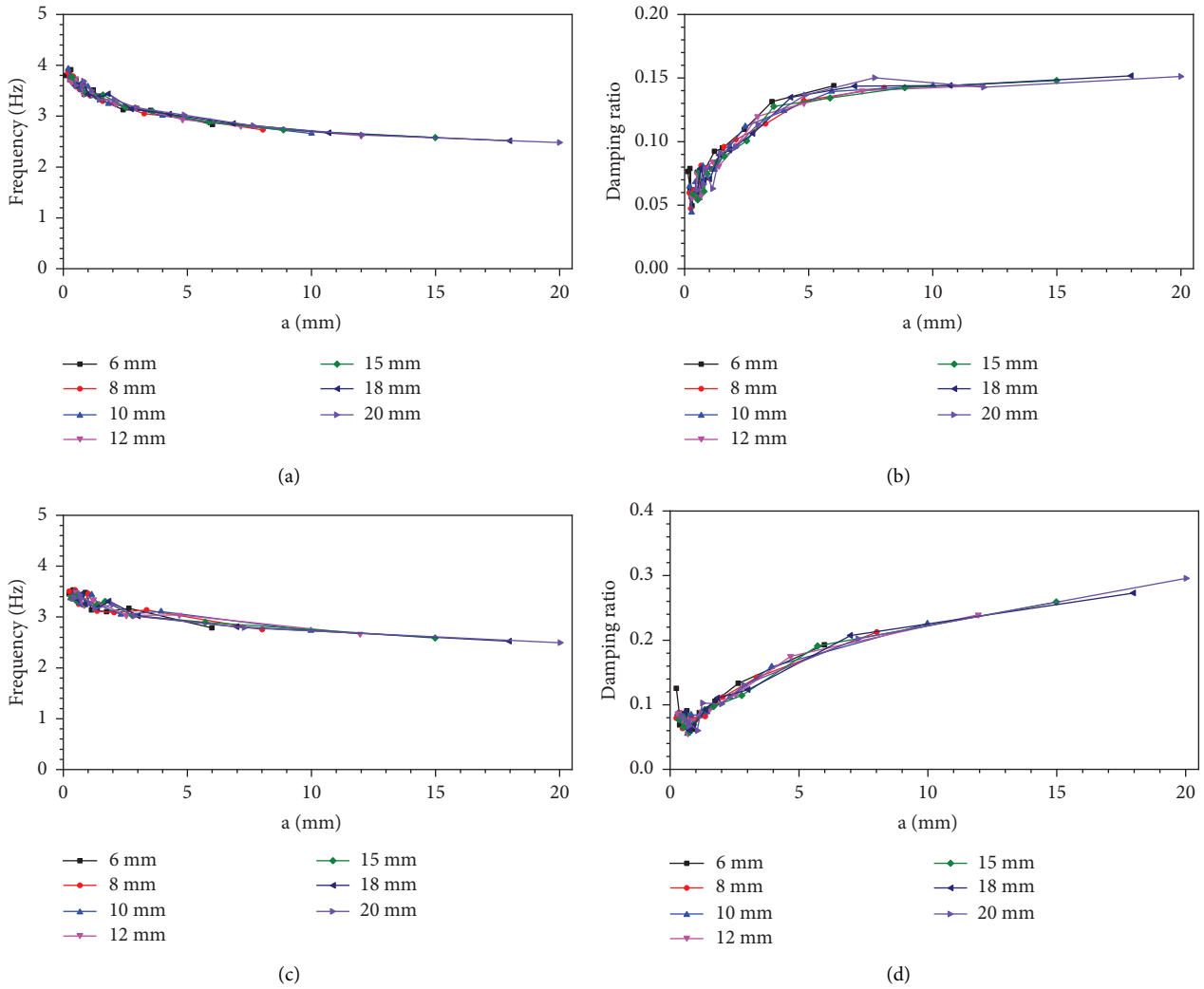

Figure 12: Summary of the 1st-order natural frequency versus amplitude relationship and damping ratio versus amplitude relationship determined by the LogDec method. (a) Natural frequency: in air. (b) Damping ratio: in air. (c) Natural frequency: in still water. (d) Damping ratio: in still water.

To fix an appropriate threshold for E_r, the range of 1%~10% is compared. Taking the 20 mm test in air as an example (the beginning 0.06 seconds data are omitted), the 1st-order natural frequency versus amplitude relationship and damping ratio versus amplitude relationship are illustrated in Figure 16 (other test results show similar behavior). The results show that (1) the nonlinear relationship of the 1st-order natural frequency versus amplitude is less sensitive to the threshold than that of the damping ratio; (2) the damping ratio increases with increasing E_r and finally approaches the saturation value; and (3) the relationship between the damping ratio and amplitude is not a monotonic function, which reveals the complex energy dissipation mechanism for the vibration.

When E_r equals 3%, the extracted nonlinear relationships of the 1st-order modal parameter versus amplitude are generally consistent with the results of the LogDec and data reduction methods, especially at low amplitudes, as shown in Figure 17 (only the results for the 20 mm test in air are shown; the other test results are similar). All test results in air and still water are summarized in Figure 18. The nonlinear relationship of the 1st-order natural frequency versus amplitude for different initial displacement tests is consistent and less dispersed than that of the damping ratio. When the amplitude is greater than 8 mm, the 1st-order modal damping ratio in air gradually approaches the saturation limit of 0.15. However, due to the different energy dissipation mechanisms in still water, the 1st-order modal damping ratio in still water does not approach a limit with increasing amplitude.

5.3. Comparison of the Test Results. The results of the LogDec, data reduction, and POD (svd) methods are averaged and summarized in Figure 19. These averaged results are less reliable at large amplitudes than at small amplitudes since there are fewer results for large amplitudes. Figure 19 clearly shows that the nonlinear relationships of the 1st-order natural frequency versus amplitude calculated by the three methods

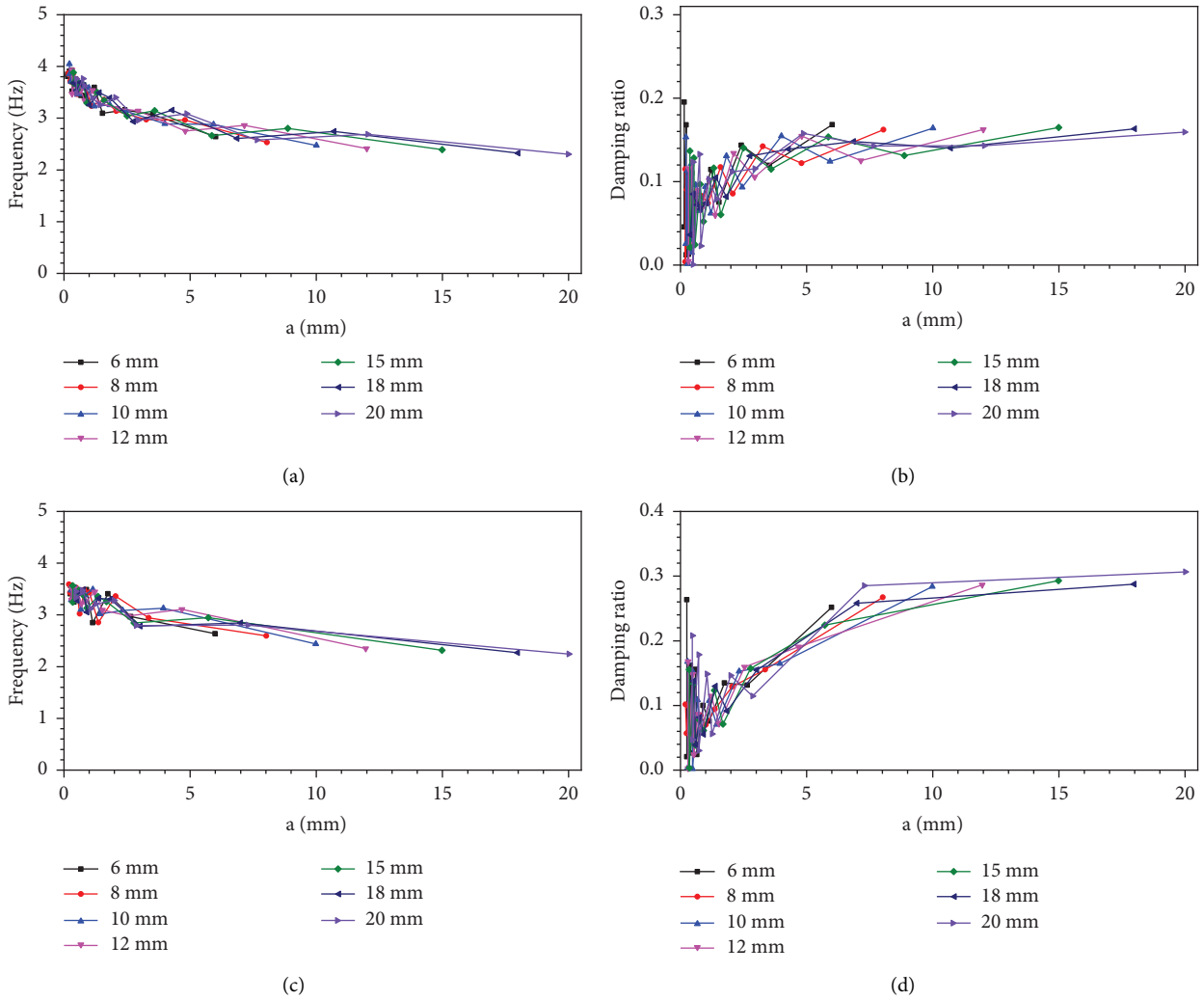

Figure 13: Summary of the 1st-order natural frequency versus amplitude relationship and damping ratio versus amplitude relationship determined by the data reduction method. (a) Natural frequency: in air. (b) Damping ratio: in air. (c) Natural frequency: in still water. (d) Damping ratio: in still water.

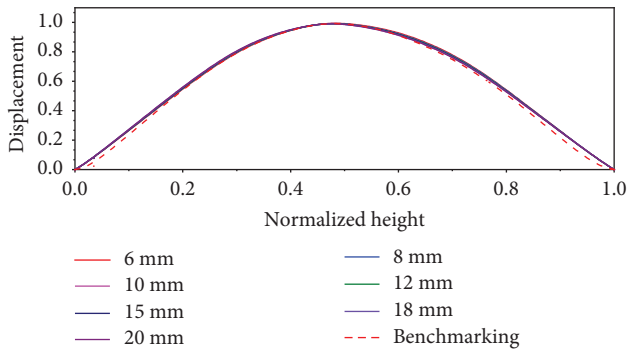

Figure 14: A comparison of the first orthogonal base $\widetilde{\Phi}_1$ to the benchmarking mode shape in air tests.

are consistent. Conversely, for the damping ratio, only the results of the LogDec and POD (svd) methods are consistent except for the data reduction method. The reasons are explained above. In the following paragraphs, only the results of the LogDec and POD (svd) methods are selected for further comparison.

Figure 19 is simplified to Figure 20 after omitting the results of the data reduction method. It is obvious that (1) the valid amplitude range for LogDec is larger than that of the POD (svd) algorithm. This is because the data in the initial 0.06 seconds are omitted by the POD (svd) algorithm. (2) The results of the LogDec and POD (svd) methods are consistent in the small-amplitude range but different in large amplitudes, and the difference becomes larger with increasing amplitude, especially in the still-water case. Deeper investigation into the LogDec method indicates that these larger-amplitude results came from the first cycle of the vibration signal. As mentioned earlier, the onset of vibration is strongly affected by static friction, and the energy dissipation mechanism differs from subsequent vibration. Therefore, for the LogDec algorithm, the larger-amplitude results are not as accurate as the lower-amplitude results. The POD (svd) algorithm shows better accuracy.

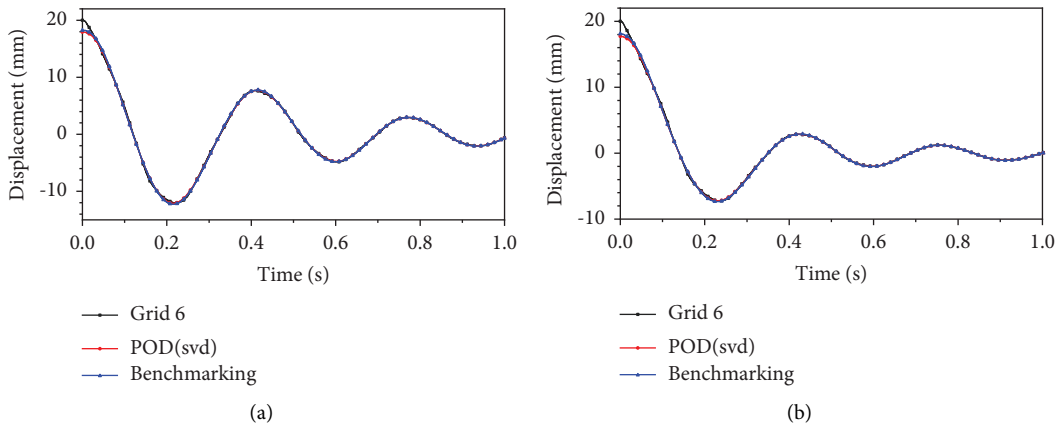

Figure 15: The separated 1st-order modal response versus grid 6 displacement time history: 20 mm test. (a) In air. (b) In still water.

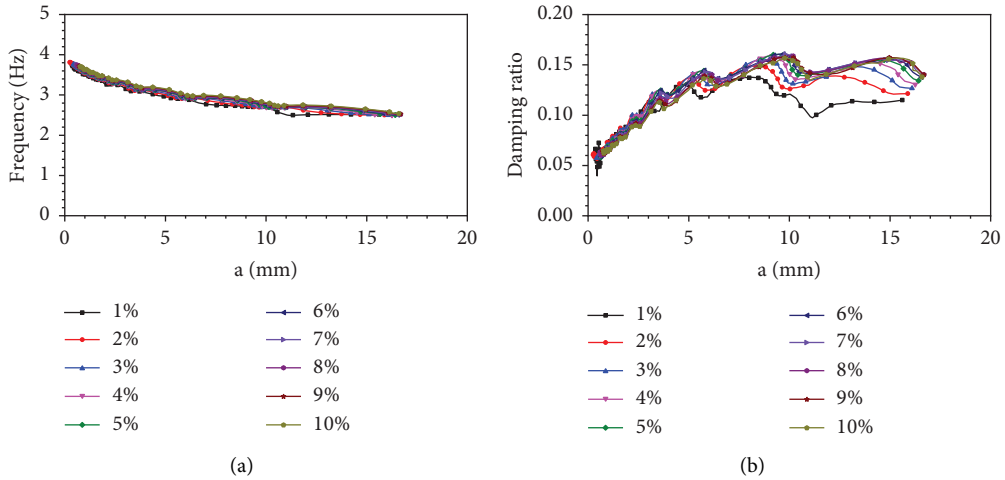

Figure 16: 1st-order modal parameters versus amplitude relationship obtained by POD (svd): 20 mm test in air; E_r: 1%~10%. (a) Natural frequency. (b) Damping ratio.

The new results of LogDec are acquired by the following steps: (1) discard the first half cycle of the vibration signal in each test; (2) based on the truncated signal, calculate the new nonlinear relationship of modal parameters versus amplitude for each test by LogDec; and (3) average all test results and then obtain new results for LogDec. The new results for LogDec and the results of POD (svd) are shown in Figure 21, and these results were almost identical, which confirms the accuracy of the POD (svd) method. Furthermore, the effective amplitude range of the results of the POD (svd) method is larger than that of LogDec, and the POD (svd) method shows more efficient data usage.

As shown in Figure 21(a), at small amplitudes, the 1st-order natural frequency in air is larger than that in still water. The difference in the 1st-order natural frequency in air and still water gradually disappears with increasing amplitude. An explanation is that when the vibration amplitude is small, the 1st-order natural frequency is much more affected by the fluid added mass effect than other factors. As the vibration amplitude increases, the sliding friction force on the contact surface between the fuel rod and grid cell increases, and its effect exceeds the fluid resistance effect. Moreover, the change in the 1st natural frequency gradually decreases and has a tendency to approach the limit value. It can also be observed from Figure 21(b) that when the amplitude is small, the damping ratios in air and still water are the same. This is because the fuel rods are stuck by the grid cells at a small amplitude, and the internal material damping force dissipates most of the vibration energy rather than fluid resistance. As the vibration amplitude increases, the damping ratio in air increases and tends to saturate. However, in still water, the damping ratio gradually increases without a limit value. The reason for this phenomenon is that the fluid resistance is proportional to the square of the velocity, which is proportional to the frequency and vibration amplitude.

5.4. Curve Fitting for the Modal Parameter Nonlinearity. To meet the needs of numerical simulation, a fractional polynomial model was used to fit the natural frequency nonlinearities and damping ratio nonlinearities in air and still water, which is expressed as follows:

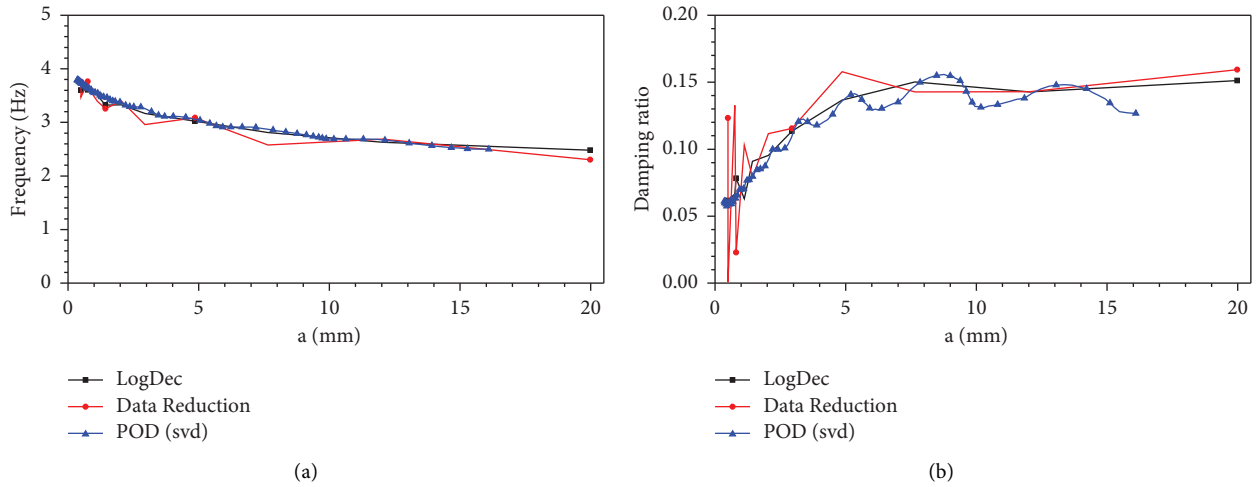

Figure 17: Comparison of results obtained by the three methods: 20 mm test in air; E_r: 3%. (a) Natural frequency. (b) Damping ratio.

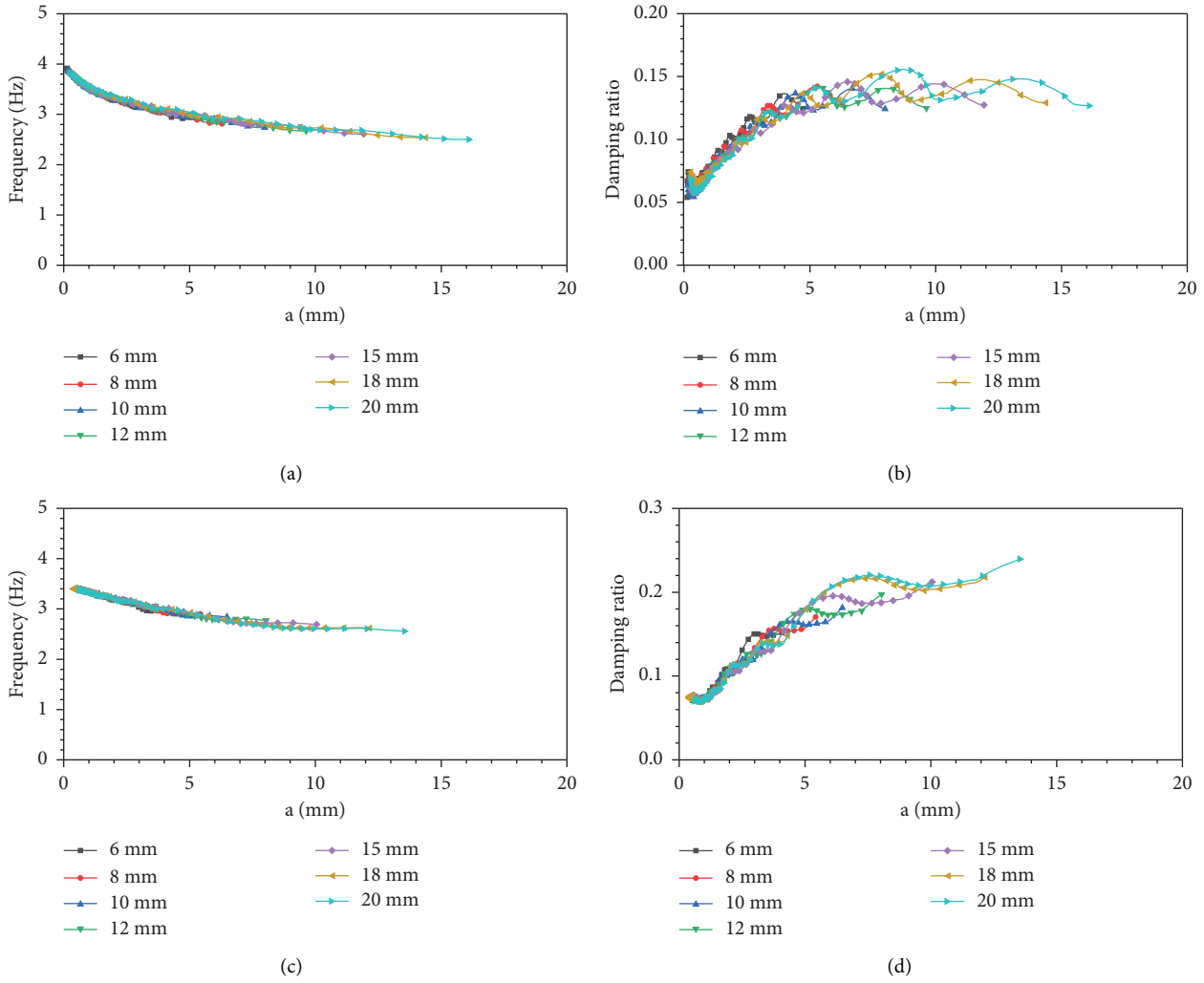

Figure 18: Summary of 1st-order modal parameters versus amplitude relationships obtained by POD (svd); E_r: 3%. (a) Natural frequency: in air. (b) Damping ratio: in air. (c) Natural frequency: in still water. (d) Damping ratio: in still water.

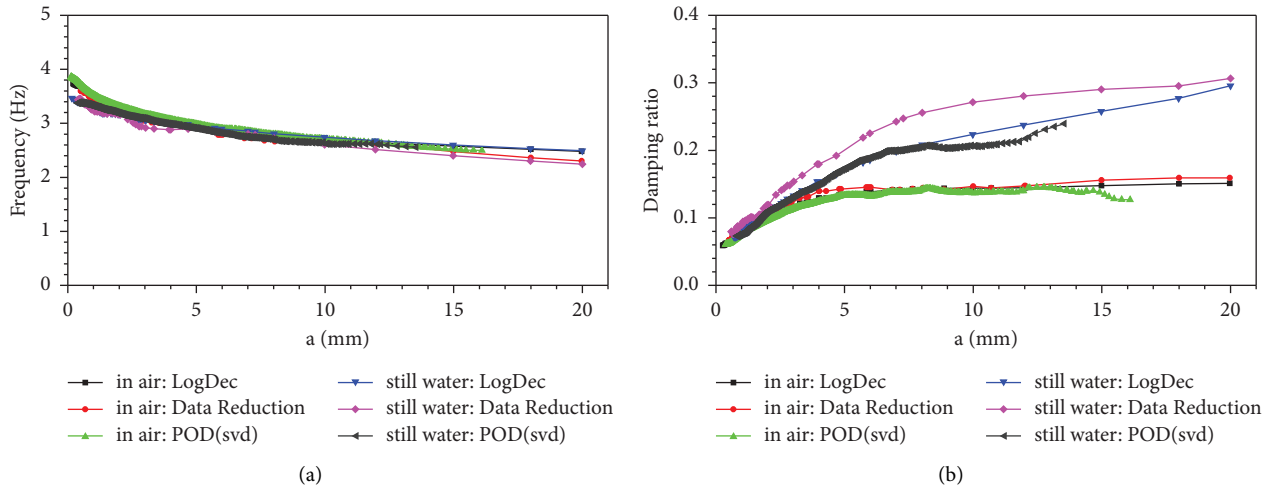

Figure 19: Summary of the 1st-order modal parameters versus amplitude relationships obtained by the 3 methods. (a) Natural frequency. (b) Damping ratio.

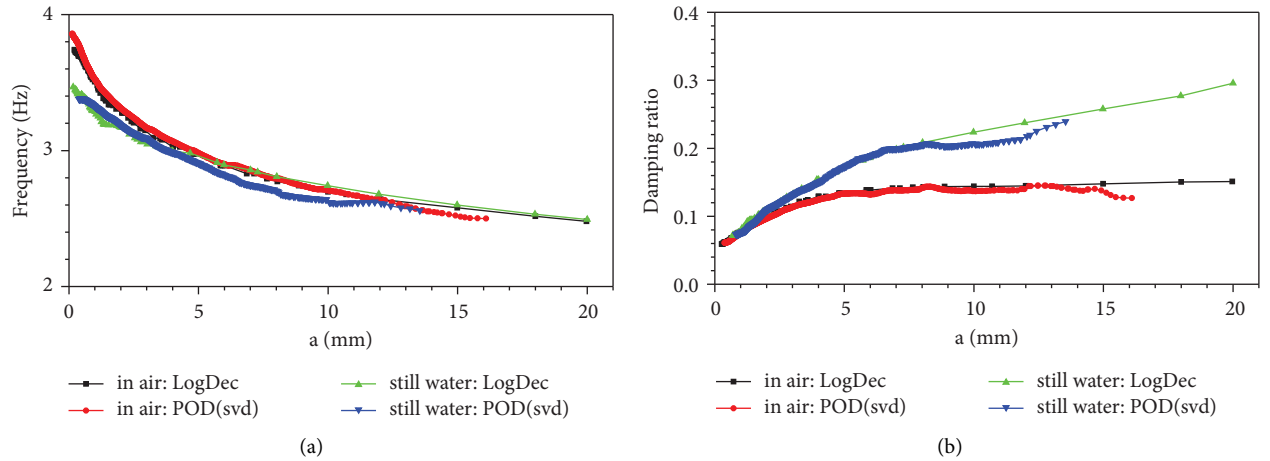

Figure 20: Summary of the 1st-order modal parameters versus amplitude relationships obtained by the LogDec and POD (svd) methods. (a) Natural frequency. (b) Damping ratio.

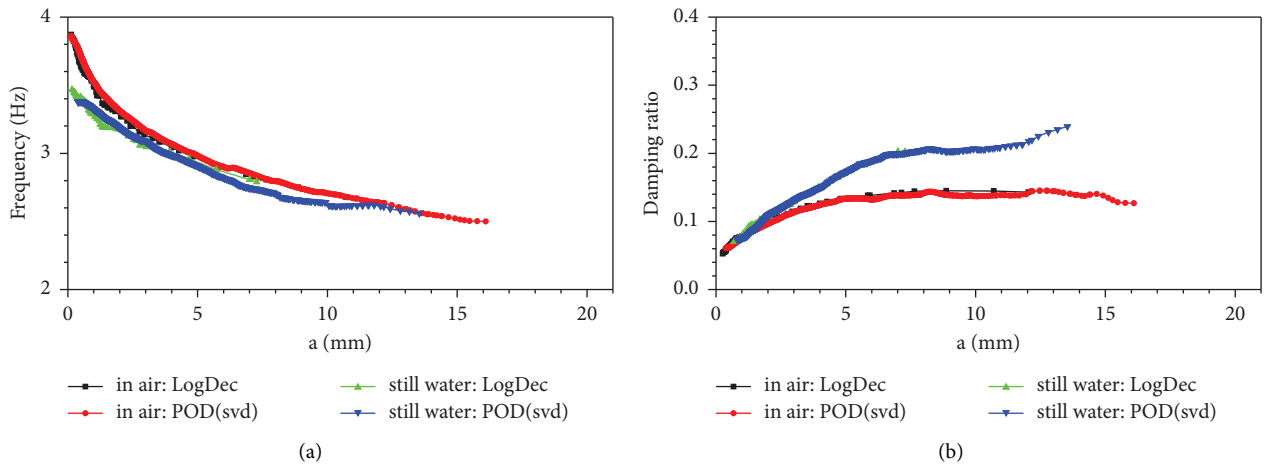

Figure 21: The new results of LogDec versus the results of the POD (svd) method. (a) Natural frequency. (b) Damping ratio.

Table 1: Fitting coefficients for the nonlinear relationship between the 1st-order natural frequency and amplitude.

Algorithm	Condition	Coefficient					R^2
		a	b	c	d	e	
POD (svd)	Air	3.956	−0.567	0.180	0.057	0.026	0.999
LogDec		3.855	−0.445	0.110	0.032	0.015	0.998
POD (svd)	Still water	3.462	−0.149	0.008	$-1.311E-04$	$-1.439E-05$	0.999
LogDec		3.525	−0.297	0.069	$1.749E-02$	$8.120E-03$	0.995

Table 2: Fitting coefficients for the nonlinear relationship between the 1st-order damping ratio and amplitude.

Algorithm	Condition	Coefficient					R^2
		a	b	c	d	e	
POD (svd)	Air	0.0488	0.0292	−0.00326	$6.782E-04$	0.00401	0.997
LogDec		0.0496	0.0305	−0.00360	$7.459E-04$	0.00415	0.999
POD (svd)	Still water	0.0431	0.0351	−0.00276	$5.884E-04$	$2.360E-03$	0.997
LogDec		0.0463	0.0365	−0.00280	$1.347E-04$	$1.858E-04$	0.993

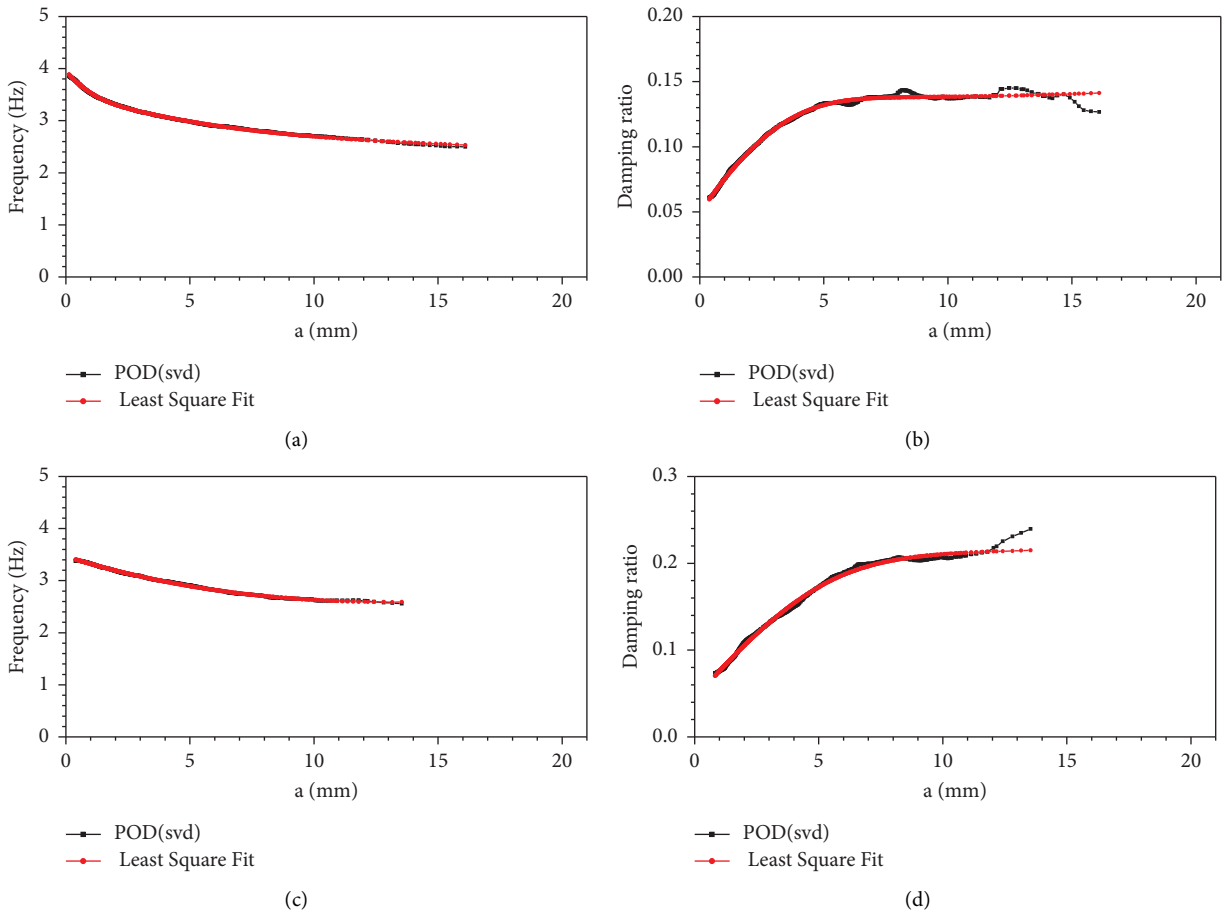

Figure 22: Least-squares fitting of the 1st-order modal parameters versus amplitude: POD (svd) method. (a) Natural frequency in air. (b) Damping ratio in air. (c) Natural frequency in still water. (d) Damping ratio in still water.

$$y = \frac{a + bx + cx^2 + dx^3}{1 + ex^3}, \tag{15}$$

where x is the amplitude in millimeters, y is the natural frequency or damping ratio, and the coefficients a, b, c, d, and e are the parameters to be fitted. It is easy to conjecture

that parameter a is the natural frequency or damping ratio close to zero amplitude. Parameter d/e is the limit of the natural frequency or damping ratio when the amplitude tends to the ultimate value.

A least-squares fit is performed for the LogDec and POD (svd) results shown in Figure 21, and the fitting coefficients are summarized in Tables 1 and 2. Figure 22 shows the POD (svd) results only. The goodness of fit is greater than 0.99, indicating a good fitting quality. Furthermore, the coefficients for the two algorithms are similar.

6. Discussion

The pluck tests combined with LogDec and data reduction are traditional SDOF structure modal parameter estimation methods and are widely used in structural dynamic mechanism tests. The requirements of LogDec and data reduction methods are summarized as follows: (1) there is only one mode excited in the fuel assembly motion; (2) the null position of the fuel assembly motion remains unchanged; (3) the fuel assembly motion meets the requirement of initial zero velocity; and (4) the energy dissipation is relatively uniform during the motion. The LogDec algorithm mainly utilizes the first cycle data, which is heavily affected by stiction. If the selection of the driving grid and initial velocity is not taken seriously, multiple modes will be excited simultaneously, greatly affecting the accuracy of the result. In contrast, the new algorithm adopts all spacer grid responses and all visible cycles and can be applied in the multimode case.

There are two aspects that need attention in the new algorithm: extracting the single-mode response from the free oscillation of spacer grids and the width of the sliding window. First, as stated in Section 4.3, there are two ways to extract the single-mode response, which have restrictions on the number and location of sensors: if the mode shapes corresponding to the sensor locations are not orthogonal with respect to the mass matrix or to themselves (not proportional to the POMs), the single-mode extraction will fail. Since the density and rigidity of the fuel assembly are uniformly distributed, these restrictions can be easily fulfilled by fixing sensors on all spacer grids. The second aspect is the width of the sliding window, which is controlled by the normalized fitting error indicator E_r. The appropriate value of E_r is determined by finding a balance between the smoothing and localizing of the nonlinear relationship between modal parameters and amplitude, which is particularly important for the nonlinearities of the damping ratio. An appropriate value of E_r makes the result of POD (svd) have the same meaning as the result of LogDec, which is not affected by the 4 restrictions described in the previous paragraphs.

7. Conclusion

The shortcomings of the LogDec and data reduction methods are discussed in detail. It is important to note that the onset of free vibration of fuel assembly is greatly affected by stiction, which is different from the continuous excitation in seismic or loss of coolant accidents. In this paper, a new identification method based on single-mode response extraction and SDOF fitting with a sliding window is proposed. The new algorithm has the following merits: (1) the nonlinear relationships between 1st-order modal parameters and amplitude are accurately extracted and show more efficient data usage; (2) the requirements of initial zero velocity and null baseline drift of motion do not need to be met; and (3) it is not only suitable for the 1st-order modal case but also applicable to the higher-order mode and multimode case. Finally, the nonlinear relationships between the 1st-order modal parameters and amplitude are fitted by a fractional polynomial, the test results are exactly fitted, the trend for the modal parameters is revealed, and the needs of numerical simulation are met.

Nomenclature

a_1: Characteristic amplitude for the first cycle
w_{n1}: Characteristic natural frequency for the first cycle
ζ_1: Characteristic damping ratio for the first cycle
w_n: Natural frequency
$T_{0.5D}$: Half damped period
ζ: Damping ratio
$y(t)$: Displacement time history
$\dot{x}_i(0)$: Initial velocity of the ith mode
$x_i(0)$: Initial displacement of the ith mode
a_i: Amplitude of the ith mode
w_{ni}: Natural frequency of the ith mode
ζ_i: Damping ratio of the ith mode
θ_i: Phase angle of the ith mode
ψ_i: Mode shape of the ith mode
M: Mass matrix
$\tilde{y}(t)$: Vector, response of the spacer grids
$\tilde{y}_{mi}(t)$: ith separated single-mode free decay response determined by Algorithm 1
$\tilde{\Psi}$: Matrix construction using $\tilde{y}(t)$
$\tilde{y}_i(t)$: Response of the ith spacer grid
$\tilde{U}$: Matrix obtained by the SVD of $\tilde{\Psi}$, containing the orthogonal base
$\tilde{S}$: Matrix obtained by the SVD of $\tilde{\Psi}$, containing a singular value
$\tilde{V}$: Matrix obtained by the SVD of $\tilde{\Psi}$
s_k: Singular value
$p_k(t)$: kth temporal evolution
P: Matrix obtained from the product of $\tilde{S}$ and $\tilde{V}^T$
$\tilde{u}_k$: kth column of the orthogonal base matrix $\tilde{U}$
$\tilde{\Phi}_k$: Vector obtained by normalizing the maximum value in $\tilde{u}_k$ to 1.0
$\tilde{y}_{mk}(t_i)$: kth separated single-mode free decay response determined by Algorithm 2
$\tilde{p}_k(t)$: Separated single-mode free decay response, proportional to $p_k(t)$
d_{ik}: Constant, compensation for the drift of the baseline
t_p: Start time of the window
Δt: Window length
t_q: End time for the window
E_r: Fitting error

$\tilde{y}_m(t)$: Separated single-mode free decay response ($\tilde{y}_{mi}$ or $\tilde{y}_{mk}$)
$y_i(t)$: Theoretical value for the separated single-mode free decay response
$DE_r(t_i)$: Normalized deformation energy ratio
y: Natural frequency or damping ratio
x: Amplitude in millimeters
a: Coefficient in the fractional polynomial model
b: Coefficient in the fractional polynomial model
c: Coefficient in the fractional polynomial model
d: Coefficient in the fractional polynomial model
e: Coefficient in the fractional polynomial model
R: Goodness of fit.

Data Availability

The data used to support the findings of this study are available from the corresponding author upon request.

Conflicts of Interest

The authors declare that there are no conflicts of interest regarding the publication of this paper.

References

[1] J. C. Queval and D. Brochard, "Analysis of Impact Phenomena between PWR Fuel Assemblies in Earthquake Situations," in *Proceedings of the ASME Pressure Vessel And Piping Conference: Vibration and Seismic Response Of Fluid-Structure Systems*, Pittsburgh, PA, USA, June 1988.

[2] B. Collard, S. Pisapia, S. Bellizzi, and F. Witters, "PWR FUEL Assembly Modal Testing and Analysis," in *Proceedings of the ASME Pressure Vessels And Piping Conference*, pp. 147–152, Cleveland, OH, USA, August 2003.

[3] Y. Roger and D. D. S. Lu, "PWR Fuel Assembly Damping Characteristics," in *Proceedings of the International Conference On Nuclear Engineering*, pp. 211–217, San Diego, Ca, USA, November 2006.

[4] S. Pisapia, B. Collard, S. Bellizzi, and V. Mori, "Modal testing and identification of a PWR fuel assembly," in *Proceedings of the Transactions of the 17th International Conference on Structural Mechanics in Reactor Technology (SMiRT 17)*, Czech, Europe, August 2003.

[5] G. Ricciardi and E. Boccaccio, "Mass, stiffness, and damping identification for a pressurized water reactors fuel assembly by a proper orthogonal decomposition method," *Journal of Pressure Vessel Technology*, vol. 136, no. 6, 2014.

[6] G. Ricciardi, "Hydraulic coupling of fuel assemblies under axial flow, confinement effect," *Nuclear Engineering and Design*, vol. 326, pp. 190–201, 2018.

[7] G. Ricciardi, "Parametric study on confinement effect on a fuel assembly dynamical behavior under axial flow," *Journal of Fluids and Structures*, vol. 78, pp. 109–125, 2018.

[8] G. Ferrari, P. Balasubramanian, S. Le Guisquet et al., "Non-linear vibrations of nuclear fuel rods," *Nuclear Engineering and Design*, vol. 338, pp. 269–283, 2018.

[9] G. Ferrari, G. Franchini, L. Faedo et al., "Non-linear vibrations of a 3×3 reduced scale PWR fuel assembly supported by spacer grids," *Nuclear Engineering and Design*, vol. 364, Article ID 110674, 2020.

[10] J. C. Flamand, J. C. Maguin, A. Mattei, J. Rigaudeau, and J. C. Leroux, "Influence of axial coolant flow on fuel assembly damping for the response to horizontal seismic loads," *SMiRT 11 Transactions*, vol. 5, pp. 139–144, 1991.

[11] P. Fardeau, D. Barbier, E. de Langre, and J. Rigaudeau, "Damping from axial coolant flow in the response of PWR fuel assemblies to horizontal seismic loads," in *Proceedings of the Transactions of the 14th International Conference on Structural Mechanics in Reactor Technology (SMiRT 14)*, Lyon, France, August 1997.

[12] Mitsubishi Heavy Industries Ltd, *Axial Flow Damping Test of the Full-Scale US-APWR Fuel Assembly*, Mitsubishi Heavy Industries, Ltd, Coimbatore, India, 2013.

[13] S. Nagarajaiah and B. Basu, "Output only modal identification and structural damage detection using time frequency & wavelet techniques," *Earthquake Engineering and Engineering Vibration*, vol. 8, no. 4, pp. 583–605, 2009.

[14] T. P. Le and P. Argoul, "Continuous wavelet transform for modal identification using free decay response," *Journal of Sound and Vibration*, vol. 277, no. 1-2, pp. 73–100, 2004.

[15] K. Dziedziech, A. Nowak, A. Hasse, T. Uhl, and W. J. Staszewski, "Wavelet-based analysis of time-variant adaptive structures," *Philosophical Transactions of the Royal Society A: Mathematical, Physical & Engineering Sciences*, vol. 376, no. 2126, Article ID 20170245, 2018.

[16] L. Zhao, D. Jin, H. Wang, and C. Q. Liu, "Modal parameter identification of time-varying systems via wavelet-based frequency response function," *Archive of Applied Mechanics*, vol. 90, no. 11, pp. 2529–2542, 2020.

[17] N. Zhao, C. Lu, M. Chen, N. Luo, and C. Q. Liu, "Parametric study of pounding tuned mass damper based on experiment of vibration control of a traffic signal structure," *Journal of Aerospace Engineering*, vol. 31, no. 6, Article ID 04018108, 2018.

[18] C. Q. Liu, D. J. Fang, and L. Zhao, "Reflection on earthquake damage of buildings in 2015 Nepal earthquake and seismic measures for post-earthquake reconstruction," *Structures*, vol. 30, pp. 647–658, 2021.

[19] R. Clough and P. Joseph, *Dynamics of Structures*, Computers & Structures Inc, Berkeley, Ca, USA, 1995.

[20] A. Preumont, P. Thomson, and J. Parent, "Seismic analysis of PWR-RCC fuel assemblies," *Nuclear Engineering and Design*, vol. 71, no. 1, pp. 103–119, 1982.

[21] H. Ward, S. Lammens, and S. Paul, *Modal Analysis Theory and Testing*, Prentice Hall inc, Katholieke Universiteit Leuven, Belgium, Europe, 1997.

[22] J. G. Béliveau, F. R. Vigneron, Y. Soucy, and S. Draisey, "Modal parameter estimation from base excitation," *Journal of Sound and Vibration*, vol. 107, no. 3, pp. 435–449, 1986.

[23] S. R. Ibrahim and E. C. Mikulcik, "A method for direct identification of vibration parameters from the free response," *The Shock and Vibration Bulletin*, vol. 47, no. 4, pp. 183–198, 1977.

[24] J. N. Juang and R. S. Pappa, "An eigensystem realization algorithm for modal parameter identification and model

reduction," *Journal of Guidance, Control, and Dynamics*, vol. 8, no. 5, pp. 620–627, 1985.

[25] G. Kerschen, J. C. Golinval, A. Vakakis, and L. Bergman, "The method of proper orthogonal decomposition for dynamical characterization and order reduction of mechanical systems: an overview," *Nonlinear Dynamics*, vol. 41, no. 1-3, pp. 147–169, 2005.

[26] G. Ricciardi, S. Bellizzi, B. Collard, and B. Cochelin, "Row of fuel assemblies analysis under seismic loading: modelling and experimental validation," *Nuclear Engineering and Design*, vol. 239, no. 12, pp. 2692–2704, 2009.